Hindawi
Geofluids
Volume 2022, Article ID 8328764, 19 pages
https://doi.org/10.1155/2022/8328764

Research Article

Experimental Study of the Flow Mechanism of Deep Lacustrine Carbonate Reservoirs in the Yingxi Area of the Qaidam Basin

Xiangrong Luo,[1] **Yongxian Zheng**,[2] **Penggang Huang**,[3] **Li'an Yang**,[3] **Xiaodong Chen**,[2] **Xiaojuan Ren**,[1] **Guo Wang**,[2] **Yanzhi Wang**,[2] **Zhiguo Wang**,[4] **and Xiaoxiao Li**[5]

[1]*Engineering Research Center of Development and Management for Low to Extra-Low Permeability Oil & Gas Reservoirs in West China, Ministry of Education, Shaanxi Key Laboratory of Advanced Stimulation Technology for Oil & Gas Reservoirs, School of Petroleum Engineering, Xi'an Shiyou University, Xi'an, Shaanxi 710065, China*
[2]*Research Institute of Exploration & Development, PetroChina Qinghai Oilfield Company, Dunhuang, Gansu 736202, China*
[3]*Oil & Gas Technology Research Institute, PetroChina Changqing Oilfield Company, Xi'an, Shaanxi 710018, China*
[4]*Mechanical Engineering College, Xi'an Shiyou University, Xi'an, Shaanxi 710065, China*
[5]*College of Petroleum Engineering, China University of Petroleum-Beijing, Beijing 102249, China*

Correspondence should be addressed to Xiangrong Luo; xiangrong_luo@163.com and Yongxian Zheng; 510816724@qq.com

Received 3 July 2021; Revised 26 October 2021; Accepted 23 December 2021; Published 1 February 2022

Academic Editor: Sohrab Zendehboudi

Many of the exploration and development theories derived for conventional clastic rock reservoirs are not applicable to pore-fracture lacustrine carbonate reservoirs. The fluid flow mechanisms under reservoir conditions are still unclear. Therefore, in this study, the rock samples were characterized using X-ray diffraction (XRD), porosity-permeability analysis, scanning electron microscopy (SEM), plain thin sections, and casting thin sections. The core samples were classified into two types (fractures and matrix pores) based on their reservoir spaces. The core flow experiments were performed under reservoir conditions using reservoir core plugs. The experimental results demonstrate that the cores, especially the fractured cores, have a strong stress sensitivity. The oil phase flow in the core has the characteristics of non-Darcy flow, and the threshold pressure gradient is 0.01–0.003 MPa/m. Additionally, for the oil-water two-phase flow in the fractured core, the water phase relative permeability of the residual oil is high. In contrast, the water phase relative permeability of the matrix core is less than 0.2. The nuclear magnetic resonance (NMR) transverse relaxation time (T_2) spectra were used to analyze the differences between the water flooding characteristics of the two pore structures. The experimental results show that the peaks of the T_2 spectra after water flooding are lower than those before water flooding, and the matrix cores have a better oil displacement effect. The relaxation time of 0.1–10 ms makes the greatest contribution to the water flooding efficiency. The micropores smaller than 10 μm in diameter play an important role in the water flooding of the matrix core. These results will provide theoretical basis for solving the difficult problems of developing deep lacustrine carbonate reservoirs.

1. Introduction

Carbonate reservoirs play an important role in global oil and gas resources [1, 2]. China is also rich in carbonate oil and gas resources. According to the dynamic evaluation results of the national oil and gas resources, the amount of geological petroleum resources is 340×10^8 t, and the amount of geological natural gas resources is 24.3×10^{12} m^3, accounting for 27.0% and 26.9% of the total oil and gas resources, respectively. Carbonate rocks can be formed in different sedimentary environments. After decades of exploration, many lacustrine carbonate reservoirs have been discovered in China and abroad [3–5]. Under the comprehensive influence of the Cenozoic paleostructure and paleoclimatic conditions, a typical plateau saline lake basin was developed in the Qaidam Basin [6, 7].

The Yingxi region is located in the northwestern section of the Yingxiong ridge, Qaidam Basin (Figure 1). The Earth's

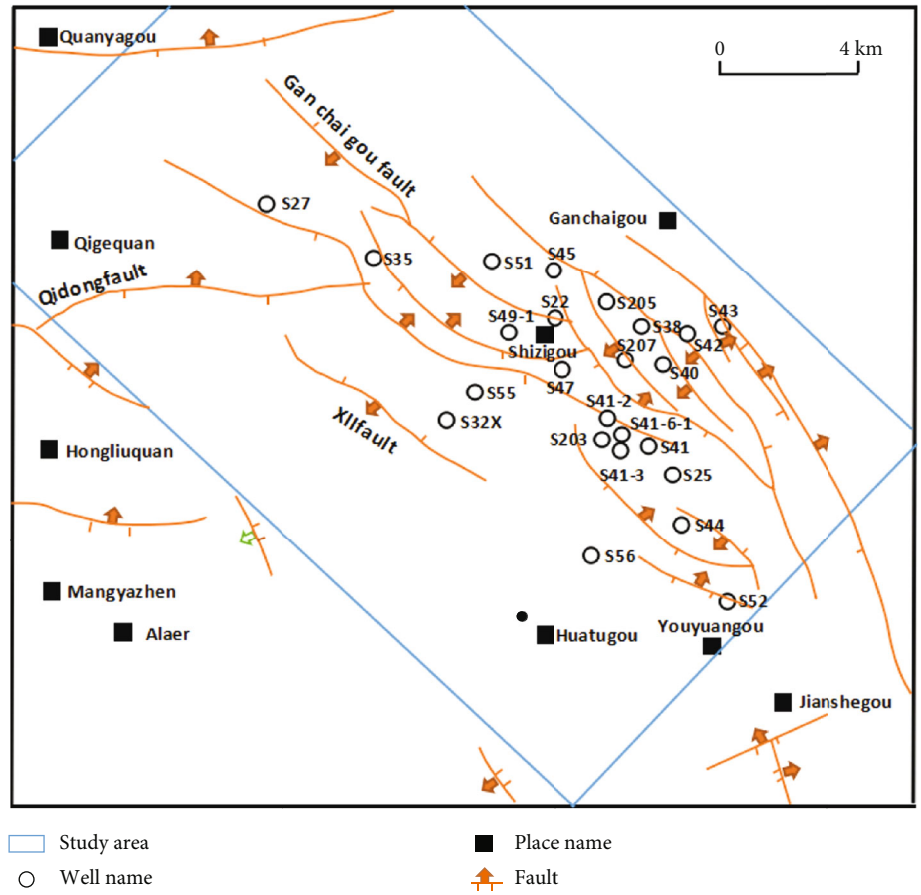

FIGURE 1: The location of the Yingxi region in the western Qaidam Basin [6].

surface is dominated by wind-eroded mountains, with ravines at altitudes of 3000–3900 m. The Yingxiong ridge tectonic belt is controlled by fold deformation, a slip fault, a basement fault, and lithologic difference; the regional trap is characterized by a large area and diverse types. The upper section of the Xiaganchaigou Formation, which is a semi-deep lake deposit, is the main oil-producing section in the deep layer in the Yingxi region, and it is also one of the best source rocks in the western Qaidam Basin [8, 9]. Combined with the saline lake basin evolution stage, the types of rocks in the upper section of the Xiaganchaigou Formation in the Yingxi region can be classified as clasolites, carbonates rocks, and evaporitic rocks. The clasolites were formed in the lacustrine dilution stage. The dark fine-grained deposits are the most common, and fewer silty fine sandstone and mudstone deposits are developed. The carbonate rocks were formed during the initial salinization of the lake water. The carbonate rocks mainly include micritic dolomitic limestone and micritic calcite dolomite, containing silty and mud terrigenous clasts. The mixed evaporites and salt rocks were formed during the transitional stage and the salinization stage of the lake water. As the climate became drier, evaporation began to outstrip the freshwater replenishment, the salinity of the lake water increased rapidly, the evaporation salt mineral content increased, and evaporites were developed, including (gray matter or dolomite) anhydrite, (gray matter or dolomite) calcium mirabilite, and salt rocks.

The E_3^2 carbonate reservoir in the Yingxi region is a high-pressure-fractured carbonate reservoir. As shown in Figure 2, it is overlain by a thick layer of salt rocks. The reservoir's pressure coefficient is 1.7–2.1. The reservoir space mainly includes intercrystalline pores in the dolomite and fractures, making this a pore-fracture reservoir [6]. In the early stage of production, the daily oil output was more than 100 tons, and then, it decreased to dozens of tons and maintained stable production for a long time. This carbonate reservoir, which is located in a saline lake basin, is controlled by the sealing of the tight salt layer, which is characterized by a strong heterogeneity, a high formation pressure, containing oil throughout, and a high local yield. Moreover, the problems of a fast decline in production and large planar differences have been encountered. Thus, it is necessary to analyze and study the flow characteristics of this reservoir in detail from an exploration point of view.

The flow mechanism of carbonate reservoirs has always been a difficult and important research topic in petroleum engineering [10–13]. Zhao et al. [14] used the rock mechanics analysis method and medium series and parallel models to establish a scale model of a stress-sensitive reservoir. Zhang et al. [15] compared five types of stress sensitivity equations via experiments and theoretical analysis and concluded that this stress sensitivity model for a fractured reservoir can be described by a power law function. However, little research has been conducted on the effects of the

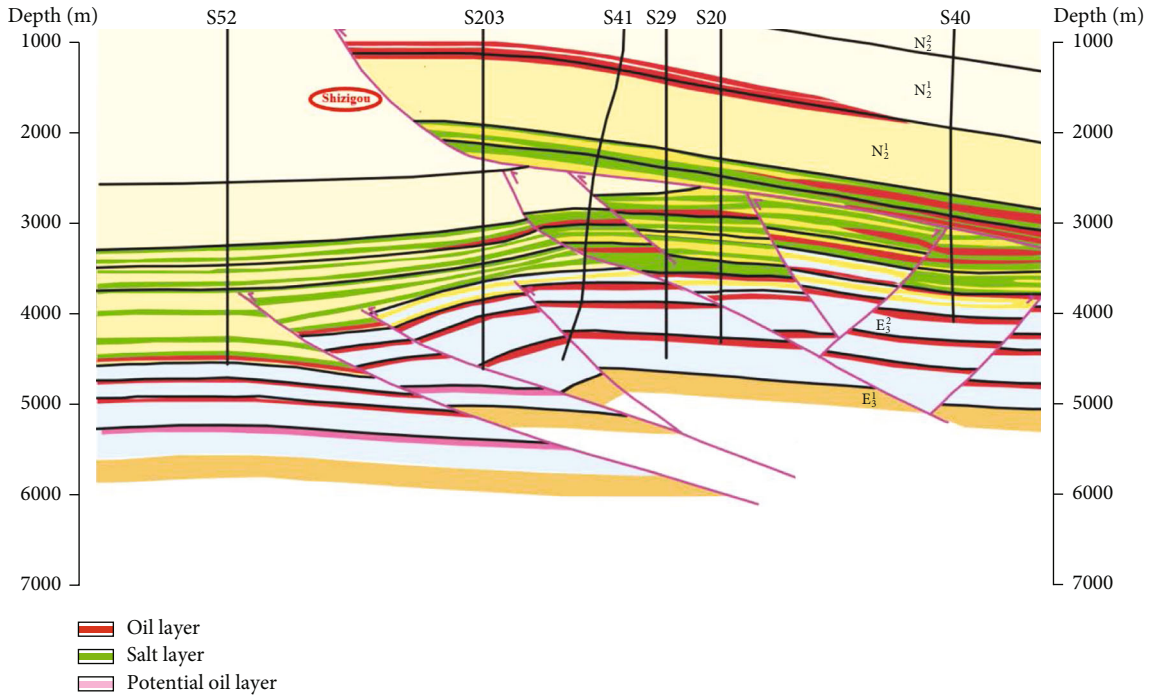

Figure 2: Geologic profile of the Yingxi deep zone.

complex pore structures of pore-fracture carbonate reservoirs on their stress sensitivity. At present, many studies have focused on fracture-cavity carbonate reservoirs. A great deal of research has been conducted on the flow mechanism, equivalent continuum, and reservoir and flow models [2, 16, 17]. However, the current research on the low-velocity flow characteristics of pore-fracture carbonate reservoirs is insufficient. Previous studies of the nonlinear flow mechanism mainly focused low permeability sandstone or shale reservoirs, and a non-Newtonian fluid, tight pores, and a boundary layer were used to explain the basic mechanism of nonlinear flow [18–22]. The low velocity flow mechanism in pore-fracture carbonate reservoirs has seldom been studied. It is unclear whether pore-fracture carbonate reservoirs have threshold pressure gradients. Furthermore, the oil and water displacement mechanism during water flooding of a pore-fracture carbonate reservoir is still unclear.

Many of the exploration and development theories derived for conventional clastic rock reservoirs are not applicable to the lacustrine E_3^2 carbonate reservoir in the Yingxi region, so it is urgent to further develop and improve these theories. In this study, first, the basic characteristics of the reservoir rocks' mineral properties, physical characteristics, and pore structure features were analyzed. Then, the oil phase flow was investigated, and the water-oil phase flow characteristics were studied. Finally, based on experimental investigations, the stress sensitivity, non-Darcy flow mechanism, and oil and water displacement characteristics were analyzed. The results of this study can not only effectively guide oil and gas exploration and deployment in the western Qaidam area, but they also provide a reference for research of other lacustrine carbonate reservoirs.

2. Experimental Methods

2.1. Samples and Materials. In this study, carbonate rock samples were obtained from the E_3^2 carbonate reservoir in the Yingxi region in the western Qaidam Basin. In the Yingxi region, the upper section of the Xiaganchaigou Formation can be divided into seven cycles (Psq1–Psq7) based on the sedimentary sequence. The E_3^2 carbonate reservoir is developed under the first set of salt layers at the top of the third sedimentary cycle (Psq3), and it is the primary high-yield strata in the upper section of the Xiaganchaigou Formation in the Yingxi region. The depths of the samples used in our experimental work ranged from 3729 to 4559 m. The samples were sealed and transported to the laboratory. In the laboratory, the samples were all drilled into columnar cores with a diameter of 2.5 cm and were washed with a mixture of benzene and anhydrous ethanol (3 : 1) in preparation for the experiments. Simulated formation water (salinity of 315,624 mg/L at 25°C) and simulated oil (density of 0.741 g/cm^3 at 25°C) were used in the experiments. The simulated formation water was prepared based on the test results for the actual formation water. The simulated oil was composed of crude oil, kerosene, and n-decane.

2.2. Core Flow Experiments

2.2.1. Experimental Setup and Conditions. As shown in Figure 3, conventional experimental core displacement equipment was used in this study. This equipment consisted of an ISCO pump, a confining pressure tracking pump, an intermediate container, a core holder unit, a flowmeter, two pressure gages, and a data collection system. Kerosene

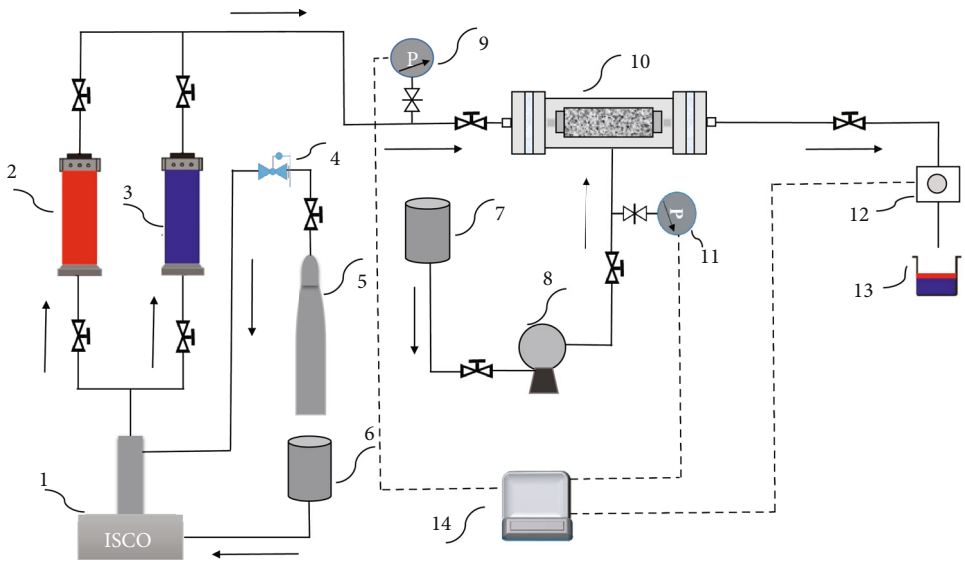

Figure 3: Schematic of the core flow experiments. Labels: 1: ISCO pump; 2: simulated oil; 3: simulated formation water; 4: pressure relief valve; 5: nitrogen cylinder; 6 and 7: kerosene tank; 8: confining pressure tracking pump; 9 and 11: pressure gages; 10: core holder; 12: flow meter; 13: effluent container; 14: computer.

was used as the working medium in the ISCO pump. The kerosene was inhaled from the inlet of the ISCO pump and pumped out from the exit to provide a driving force. Nitrogen was used in the pneumatic valves of the ISCO pump. In the course of the experiment, the simulated formation water or simulated oil that was preinstalled in the intermediate container was pressurized and injected into the core in the core holder unit using the ISCO pump. The pressure gage and flowmeter were connected to a computer to monitor and record the changes in the inlet pressure and outlet flow of the core holder unit. The system's pressure could reach 100 MPa.

Since the pressure of the E_3^2 carbonate reservoir is high under the formation conditions, the overburden pressure is also high. The effective stress can reach 30 MPa according to calculations based on test data. Thus, the experiments were needed to be performed with a suitable effective stress on the core sample in order to stimulate the actual reservoir conditions. In this study, the confining pressure reached a maximum of 30 MPa.

2.2.2. Experimental Procedures. First, flow experiments using single-phase oil were conducted under different effective stress conditions to obtain the change rule of the oil phase permeability of the core sample. The experiment proceeded as follows. (1) The core was dried in a drying oven at 80°C for 12 hours. (2) The gas permeability of the core was measured using N_2 with a purity of greater than 99.9%. (3) After the core sample was placed in vacuum for 12 hours, the simulated oil was injected into the core. (4) An electronic balance was used to weigh the core saturated with simulated oil, and its porosity was calculated. (5) The core was placed in the holder, and the confining pressure tracking pump was used to apply the confining pressure. (6) The ISCO pump was opened to set the displacement pressure. (7) The ISCO pump and data collection system were started. (8) Under a constant displacement pressure, the confining pressure was continuously increased within the interval of 3–5 MPa. Each confining pressure point was maintained for more than 30 minutes, and the oil phase permeability was measured until the confining pressure reached 30 MPa. Next, the flow curve of the core was measured to analyze the threshold pressure gradient and to study the flow characteristics of the oil phase. The initial displacement pressure was generally set to 5–8.5 MPa, and the confining pressure was 30 MPa. The confining pressure and displacement pressure should decrease synchronously. The descending interval of the two should be the same. Generally, the descending interval was 0.5–1 MPa. That is, under constant effective stress on the rock sample, the relationship between the flow and the pressure gradient was measured until the displacement pressure dropped below 0.5 MPa. Finally, the water flooding experiment was carried out to investigate the two-phase oil-water flow. Before and after the water flooding, the NMR T_2 spectra of the cores saturated with simulated oil were obtained. During the displacement, the oil, water, and cumulative fluid production were recorded accurately. When the water cut reached 99.95%, the water phase permeability under the residual oil saturation was measured, and the experiment was completed.

In addition to the flow experiments, the samples were also sent for related tests. The mineral composition was evaluated using a D/max-2500 X-ray diffractometer (XRD). Scanning electron microscopy (SEM) was conducted on plain thin sections and casting thin sections in order to observe and analyze the mineral and pore characteristics. In this study, NMR measurements were used to obtain the microscopic pore structure and the oil-water distribution characteristics. The specific methods are described in detail below.

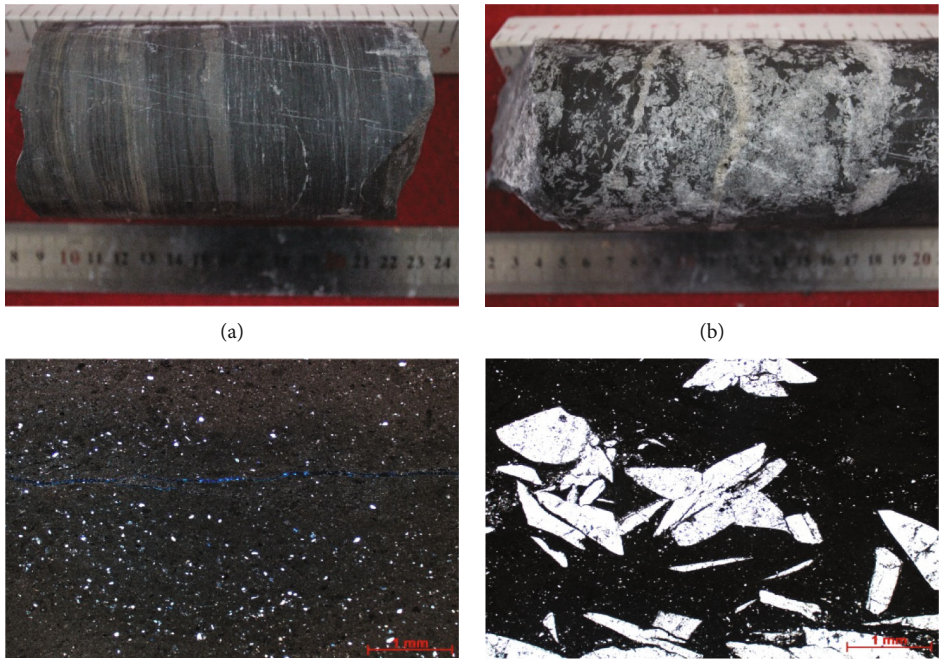

(a) (b) (c) (d)

Figure 4: Petrological characteristics of the reservoir rocks. (a) Dolomitic mudstone, sampling depth of 4138 m, (b) calcite dolomites with gypsum, sampling depth of 3731 m, (c) silty mudstone with dolomite, and (d) dolomicrite with gypsum.

2.2.3. Theory of NMR Measurements. NMR records the relaxation times of hydrogen protons in static and pulsed magnetic fields [23], and the petrophysical properties (porosity, pore size distribution, permeability, and fluid status) of rocks can be evaluated via NMR [24–26]. There is a correspondence between the T_2 relaxation time and the pore radius r. At present, the conversion between the transverse relaxation time and the pore throat radius obtained via mercury intrusion experiments is mainly conducted using the theoretical formula $r = CT_2^n$ [27–31]. In this study, according to the research results of Lai et al. [32], we evaluated the pore structure and determined the oil-water displacement characteristics of different types of pore spaces.

3. Experimental Results

3.1. Reservoir Characteristics and Classification

3.1.1. Lithology and Mineral Composition. Overall, E_3^2 is a semideep lake fine-grained sedimentary facies with a weak water energy. As shown in Figure 4, its lithology is mainly gray and black fine-grained peperite, which is one of the main hydrocarbon source strata in the western Qaidam Basin. Under the comprehensive control of the tectonic and climatic factors, many rock types, such as mudstone, limestone, and dolomite, were formed during the periodic changes in the nature of the lake water. The horizontal laminae are well developed. Evaporite minerals are generally developed in or interbedded with the dark fine-grained sediments. A large amount of strawberry pyrite, which is produced in reducing environments, was developed. As can be seen from Table 1, the mineral compositions are very complex. The abundant minerals include dolomite, feldspar, quartz, and clay minerals. The dolomite content is the highest, reaching 72.8%. Soluble minerals, such as glauberite, gypsum, and halite, were found in some of the rock samples.

3.1.2. Physical Characteristics. As shown in Figure 5, the permeability and the porosity of the reservoir have wide distribution ranges. The permeability refers to the gas permeability of the samples. The porosity of the reservoir is 0.3–16.3%. The permeability is $0.0269 - 324 \times 10^{-3}\ \mu m^2$. Overall, in the study area, the reservoir's permeability is low, and the reservoir can be classified as a low-permeability tight carbonate reservoir. The test results show that the naturally fractured cores have a high permeability. In contrast, the permeabilities of the matrix cores are small, and most of them have permeabilities of less than $1 \times 10^{-3}\ \mu m^2$.

3.1.3. Pore Structure Characteristics and Classification. The reservoir space is mainly composed of intergranular pores, intergranular dissolution micropores, macropores (residual pores), and fractures. As can be seen from Figures 6(a) and 6(d), the carbonate and clay minerals contain a large number of intercrystalline pores and intercrystalline dissolution micropores, which are the main types of reservoir space and are widely developed. As shown in Figure 6(e), the residual pores are mainly the pores formed by the incomplete filling of the structural fractures, which have a low degree of development and a high availability and are almost full of oil. In addition, the fractures are also well developed and are structural microfractures with conjugate characteristics and good connectivity (Figures 6(b) and 6(c)). It was also found that some of the fractures are filled with gypsum

Table 1: Mineral compositions of the samples.

Sample	Mineral composition (wt.%)							
	Dolomite	Feldspar	Calcite	Anhydrite	Quartz	Glauberite	Clay minerals	Others
Sy36	49.6	2.5	25.1	11.6	2.7	N/D	4.6	3.9
Sy2	25.0	12.3	13.8	N/D	12.0	N/D	29.7	7.2
Sy35	28.1	14.8	N/D	3.0	6.1	31.1	16.9	-
Sy30	62.3	6.7	N/D	1.0	6.2	N/D	20.5	3.3
Sy27	45.8	10.8	8.7	4.2	9.2	5.6	12.4	3.3
Sy42	72.8	9.7	N/D	1.6	10.9	N/D	5.0	-
Sy29	38.5	10.5	9.8	1.1	12.9	5.3	18.3	3.6
Sy21	23.5	16.3	16.5	5.4	12.6	N/D	20.2	5.5
Sy18	5.1	9.8	29.5	1.5	26.6	N/D	24.2	3.3

N/D: not detected. Others include pyrite, gypsum, and halite.

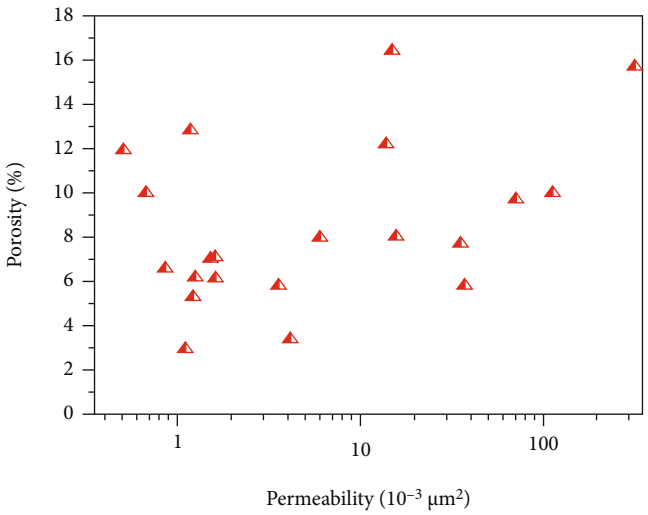

Figure 5: Plot of porosity vs. permeability for the carbonate reservoirs.

(Figure 6(f)). Figures 6(g) and 6(h) are thin section images of the matrix pore throats. Considering the complexity of the lithology and pore structure of the reservoir and the differences in the flow characteristics arising from this, based on the core observations and petrological characteristics, the reservoir space can be classified into two types: fractures and matrix pores (Table 2).

3.2. Oil Phase Flow Law

3.2.1. Permeability under Different Stress Conditions. The Yingxi E_3^2 reservoir is deeply buried, and the effective stress on the carbonate rocks is high. Therefore, the permeability under different stress conditions during the oil flow process was tested and analyzed. Two fractured and two matrix cores were selected for the oil phase flow experiments under different stresses. As shown in Figure 7, the oil phase permeability decreases with increasing effective stress. The oil phase permeability decreases exponentially. Thus, an exponential function was used to fit the experimental data, and the fitting correlation coefficient is greater than 0.98. The variations in the permeabilities of the fractured and matrix cores exhibit significant differences. The permeabilities of the fractured cores decrease faster than those of the matrix cores. Furthermore, the oil phase permeabilities of the fractured cores are more sensitive to stress.

3.2.2. Flow Curve and Threshold Pressure. The flow curve represents the relationship between the displacement pressure gradient and the flow velocity and is a direct reflection of the flow equation. Under the simulated overburden pressure of the actual reservoir, the oil phase flow curves of the four cores were determined, and the corresponding flow curves were obtained. As can be seen from Figure 8, none of the oil phase flow curves is a straight line, i.e., they are all curves. In order to further determine the flow law, the relationship between the permeability and the pressure gradient was obtained using Darcy's equation. Figure 9 shows that the oil permeability decreases as the pressure gradient decreases, which indicates that the single-phase oil flow has the characteristics of non-Darcy flow. Furthermore, the dimensionless permeability was obtained by dividing the apparent permeability value (K_o) at each point by the maximum apparent permeability value (K_{max}) of the curve, and then, the relationship between the dimensionless permeability and the pressure gradient was analyzed (Figure 10). The smaller the dimensionless permeability, the more serious the effect of the pressure gradient on the single-phase oil flow. Therefore, the decrease in the pressure gradient may be the main reason for the decrease in well production.

The low velocity non-Darcy flow equation for a single-phase fluid has many forms. For example, the modified Darcy's equation describes non-Darcy flow due to a pseudo-threshold pressure gradient [33]. More complex flow equations have also been derived, and they can describe the nonlinear part of the flow [27, 34–37]. Power functions were obtained by matching the nonlinear part of the experimental data [27, 34]. In summary, these equations are power functions, exponential functions, or linear functions with multiple parameters. In this study, by matching a large number of single-phase fluid flow experimental data, we determined a reasonable low velocity flow equation for a single-phase fluid:

$$y = ae^{-x} + bx + c, \quad (1)$$

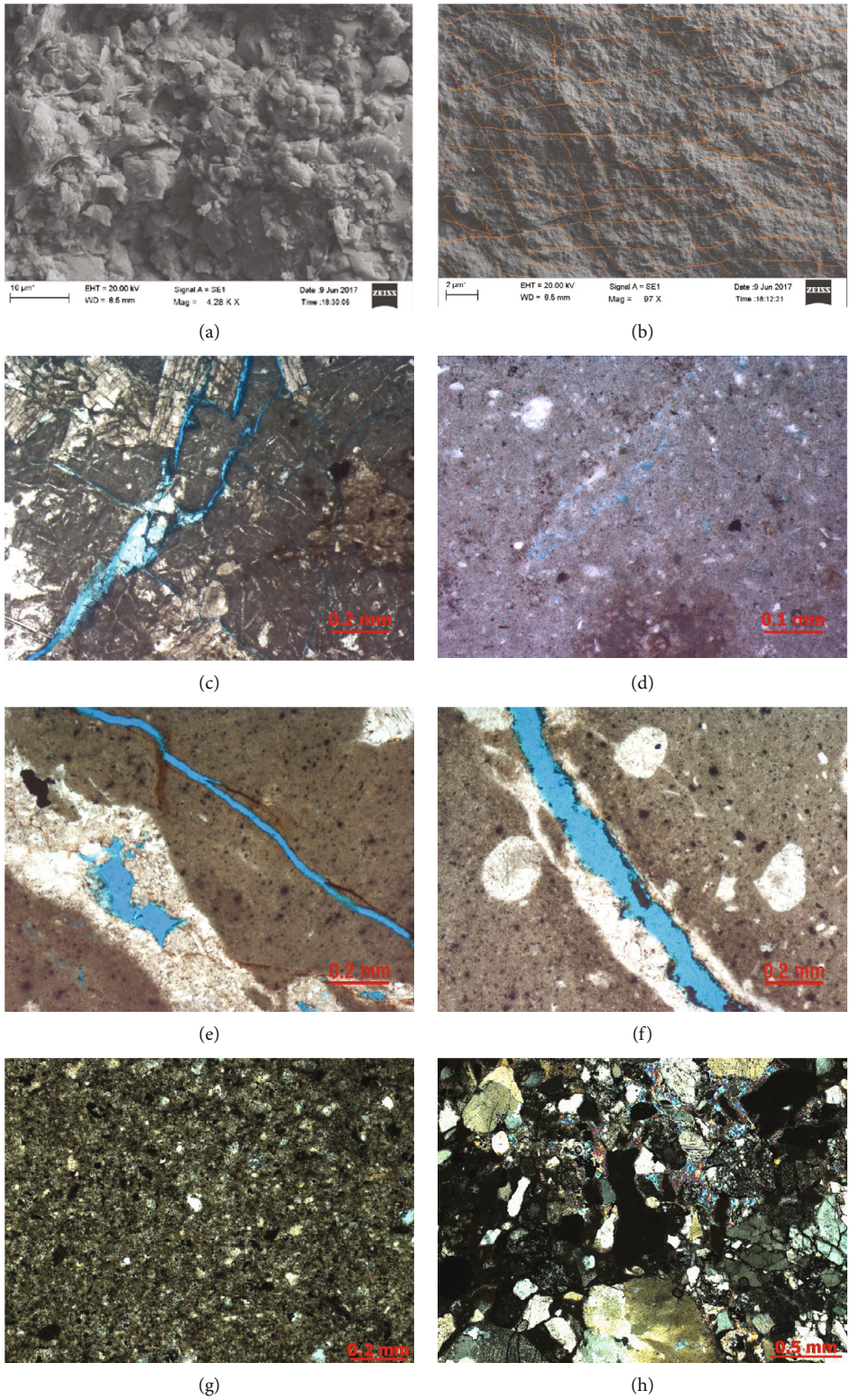

(a) (b) (c) (d) (e) (f) (g) (h)

Figure 6: Pore structure of the carbonate reservoirs. (a) Sy35, carbonate and clay mineral intercrystalline pores; (b) Sy30, micro-nano conjugate fractures; (c) Sy60, complex microfractures; (d) Sy42, dissolution pores; (e) Sy18, fracture and residual pores; (f) Sy2, fracture filled with gypsum; (g, h) Sy29 and Sy27, thin section analysis of the matrix pore throats.

where y is the experimental flow rate (mL/min); x is the pressure gradient (MPa/m); and a, b, and c are the fitting parameters. a and c reflect the influence of the fluid at the boundary layer on the flow when the core permeability is low and the pore throats are small. b is the Darcy flow coefficient, which is related to the permeability of the core and the viscosity of the fluid.

For the four cores, according to the obtained flow fitting equation, the pressure gradient value was calculated when

Table 2: Classification of the core samples' storage and flow spaces.

Sample No.	Ka (10^{-3} μm^2)	Porosity (%)	Type of pore structure	Description
Sy60	112	9.9	Fractures	Brown-gray, lime-bearing mudstone or dolomicrite, fractures developed and half-filled with crystalline salt, partially filled with gypsum.
Sy30	1.68	7.8		
Sy21	1.17	9.7		
Sy18	1.69	12.8		
Sy2	0.679	10.0		
Sy29	0.434	5.9	Matrix pores	Gray dolomicrite, hard, brittle. Gypsum or calcium mirabilite fills the cores. Intergranular pores and dissolution pores are developed.
Sy36	0.115	6.1		
Sy35	1.21	5.3		
Sy27	0.852	6.5		
Sy42	1.50	7.0		

Ka: gas permeability of the core sample.

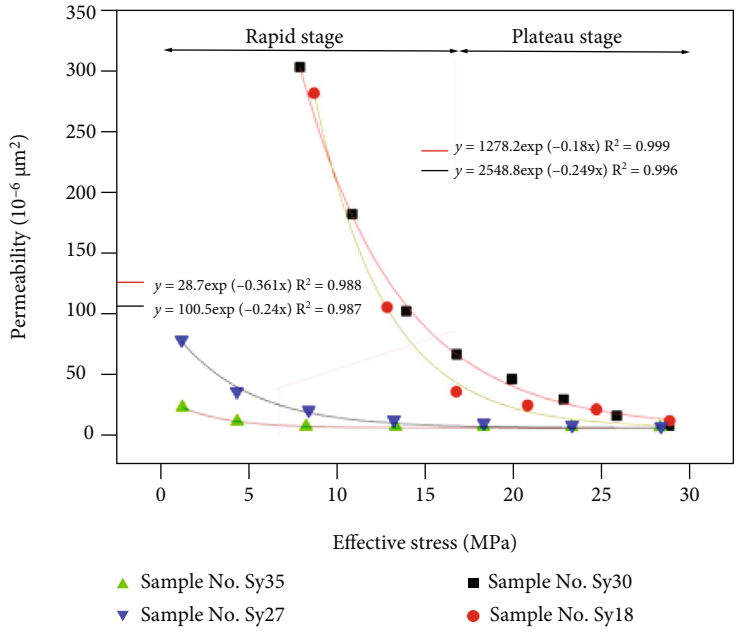

Figure 7: Plot of the oil phase permeability vs. effective stress. Sy30 and Sy18 are fractured cores; and Sy35 and Sy27 are matrix cores.

the flow rate was zero, and based on this, the threshold pressure gradients of the cores were obtained. The results are shown in Table 3. Under the effective stress of the reservoir, the cores with different types of pore structures have different threshold pressure gradients. The threshold pressure gradient of the fractured core is basically similar to that of the matrix pore core.

3.3. Oil-Water Two-Phase Flow

3.3.1. Oil and Water Relative Permeability. The relative permeability is the ratio of the effective permeability of each phase to a reference permeability when multiphase fluids coexist. The relative permeability is actually the dimensionless effective permeability, which allows for the comparison of the ratio of the flow capacity of each phase to that of a single phase. The oil and water relative permeability curves of the core samples are shown in Figure 11. There is a certain relationship between the morphology of the oil-water permeability curve and the type of pore structure. For the fractured cores, the oil phase permeability decreases sharply with increasing water saturation. The water phase relative permeability when there is residual oil is large. The saturation range of the two-phase flow zone is narrow, with an average of 11.1%. For the matrix pore cores, the saturation of the oil-water two-phase flow zone is 14.8–27.1%. The water phase relative permeability when there is residual oil is less than 0.2. The water saturation at the isosmotic point is higher. The rate of decrease of the oil phase permeability is slower. Thus, the influence of the type of pore structure on the oil-water two-phase flow is significant.

3.3.2. Analysis of NMR Results. The NMR T_2 spectra before and after water flooding are shown in Figure 12. The blue T_2 in Figure 12 represents the initial saturated oil, and the red

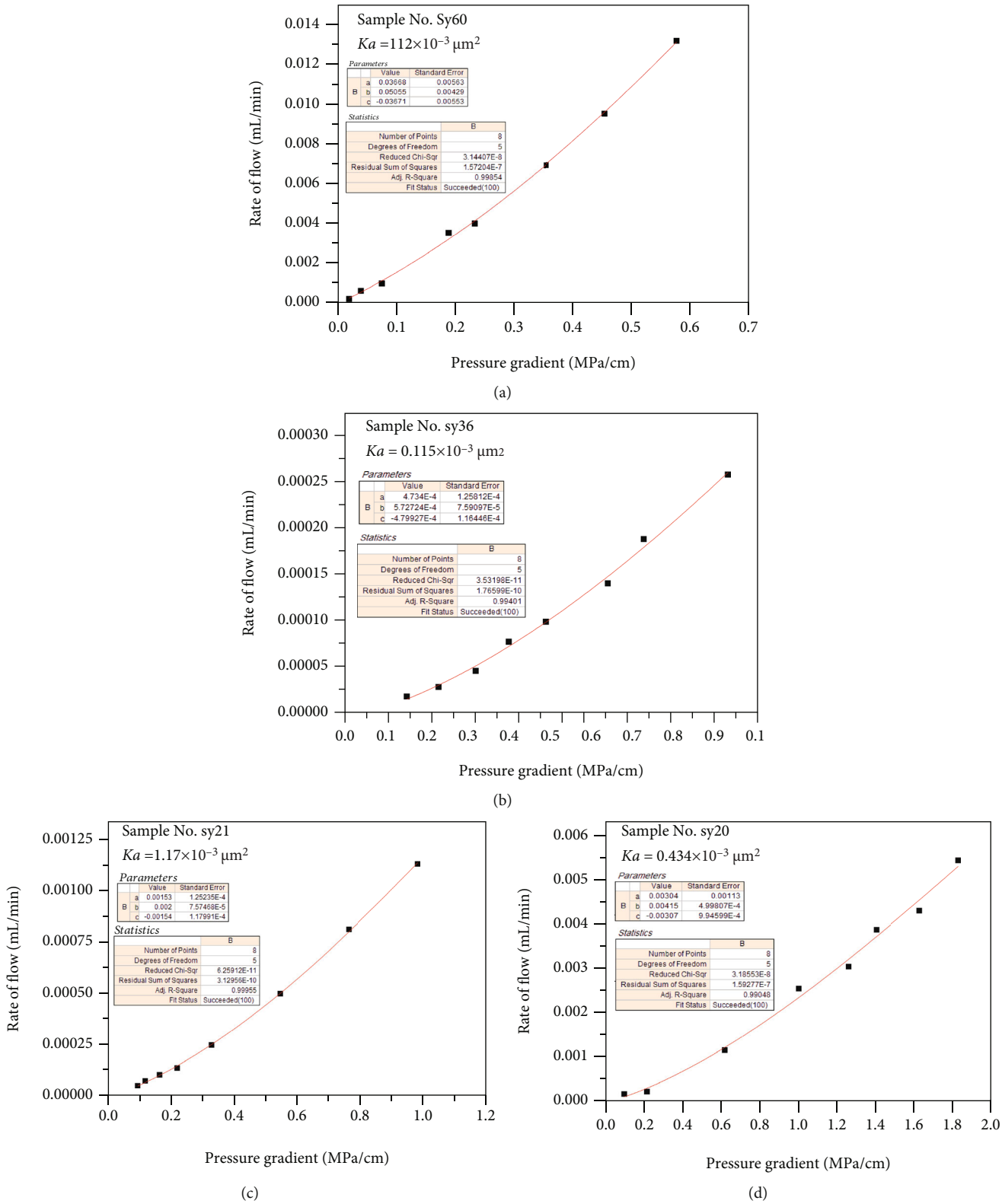

FIGURE 8: Flow curve of the oil phase in the core samples under the same stress. The relationship between the flow velocity and the pressure gradient is shown. Sy60 and Sy21 are the fractured cores, and Sy36 and Sy29 are the matrix cores.

T_2 shows the residual oil distribution after water flooding. It can be seen that the NMR T_2 spectra are mainly characterized by bimodal distributions and are mostly left-skewed. As mentioned above, NMR can be used to evaluate the pore structures of rocks. The larger the NMR T_2 value, the larger the corresponding pore throat size [38, 39]. Lai et al. [40]

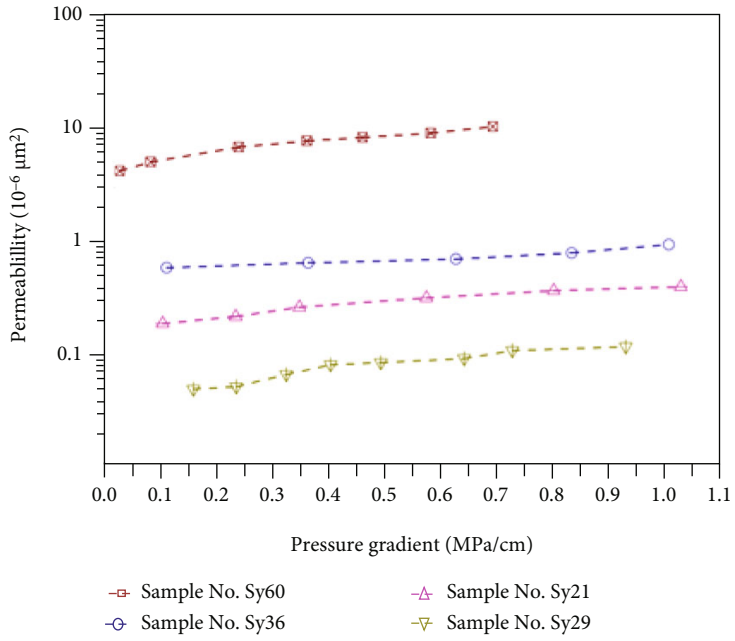

Figure 9: Plot of the oil phase permeability vs. pressure gradient. The permeability increases as the pressure gradient increases.

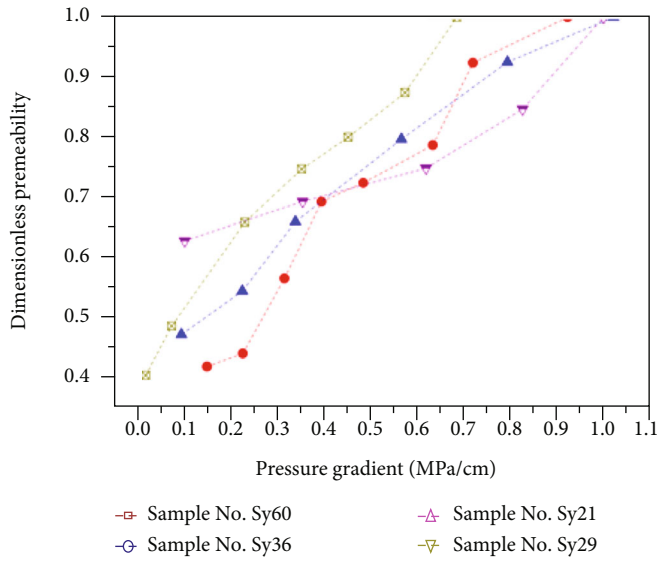

Figure 10: Plot of the dimensionless permeability vs. pressure gradient. The dimensionless permeability is the ratio of the apparent permeability to the maximum apparent permeability.

Table 3: Threshold pressure gradients of the cores with different pore structures and their fitting parameters.

Pore structure	Sample No.	Ka (10^{-3} μm^2)	Fitting parameters × 10^3			Threshold pressure gradient (MPa/cm)
			a	b	c	
Fractures	Sy60	112	36.68	50.55	36.71	0.00216
	Sy21	1.17	1.53	2.00	1.54	0.0205
Matrix pores	Sy36	0.115	0.473	0.573	0.480	0.0579
	Sy29	0.434	3.04	4.15	3.07	0.0261

Ka: gas permeability of the core sample.

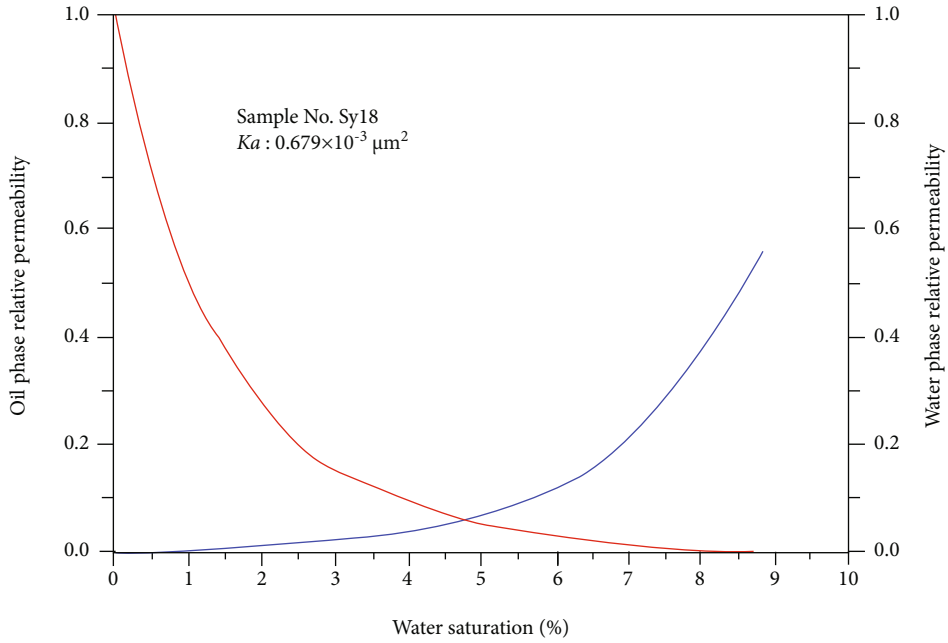

(a)

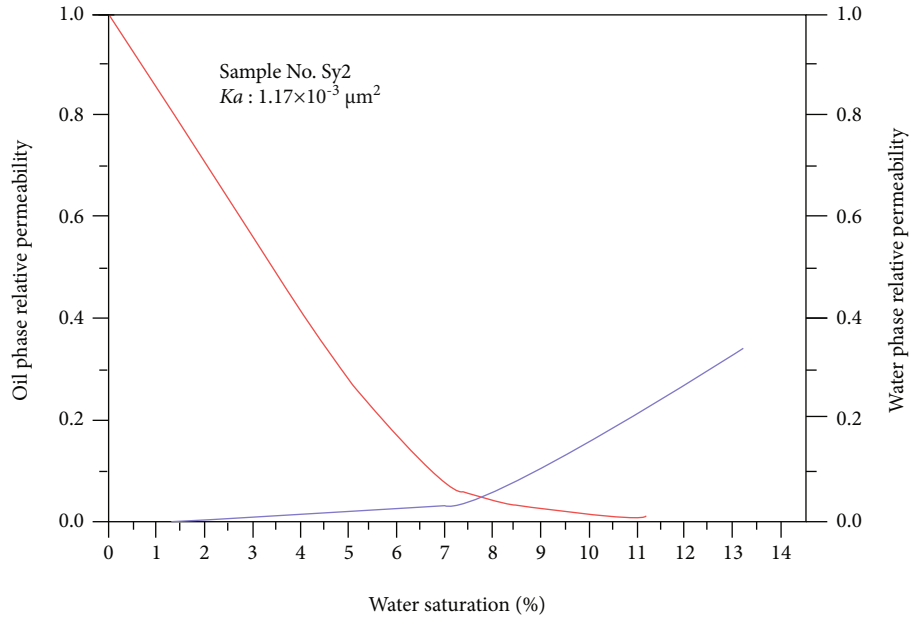

(b)

Figure 11: Continued.

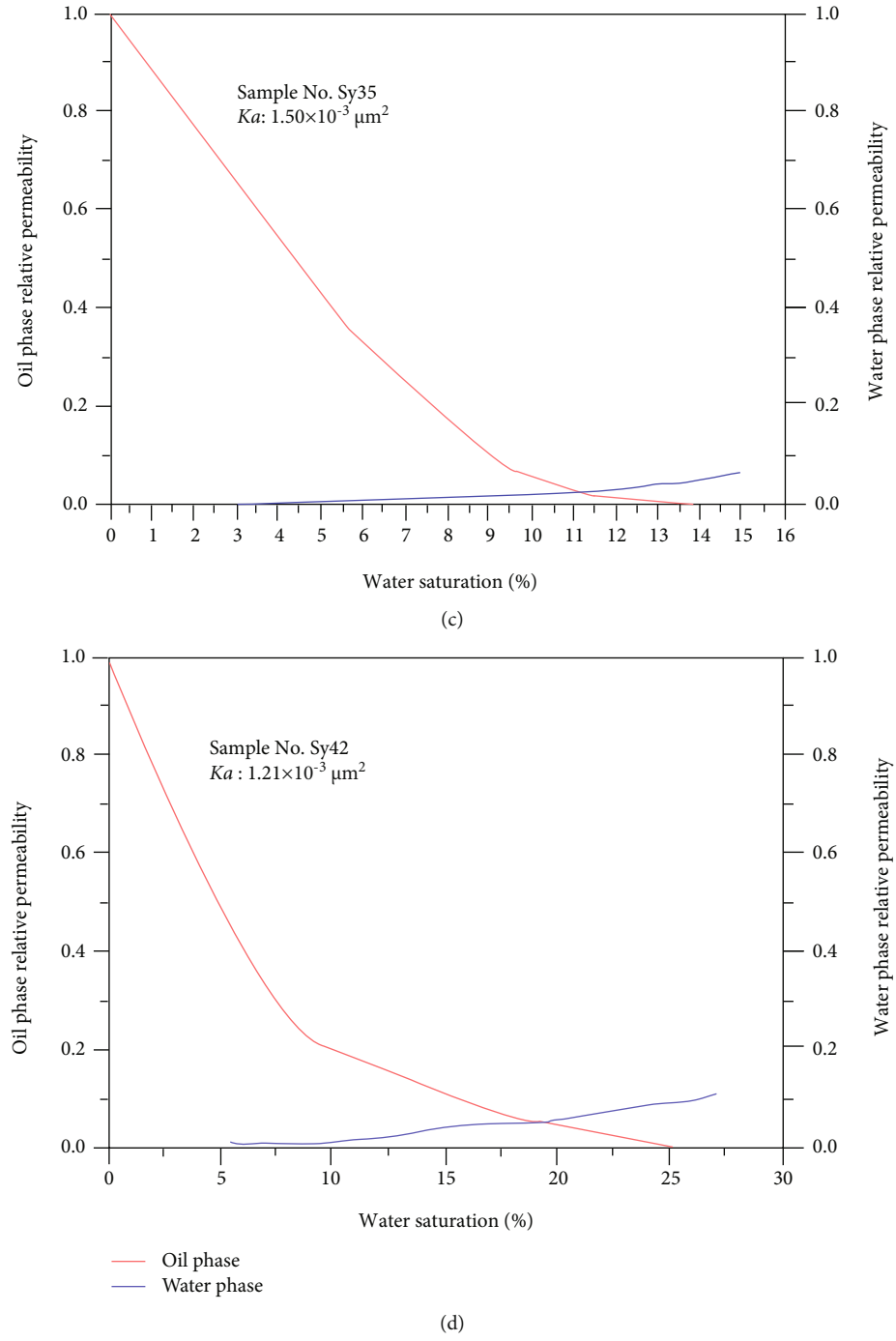

Figure 11: Oil-water relative permeability curve. Sy18 and Sy2 are fracture type, and Sy35 and Sy42 are matrix pore type.

found that the very low T_2 components (<50 ms) are associated with small intracrystalline pores (<10 μm). In this study, the left peaks with T_2 components ranging from 0.1 ms to 10 ms are related to the <10 μm intracrystalline and intergranular pores. Thus, it is concluded that lacustrine carbonate reservoirs mainly develop micropores, and macropores are less abundant. The right peaks with T_2 components ranging from 10 ms to 500 ms are related to the intercrystal pores and dissolution pores with pore sizes ranging from several microns to about 100 μm. Previous studies have shown that microfractures have tailed T_2 distributions. In carbonates, the signals of long T_2 components (>1000 ms) in NMR measurements originate from microfractures or vugs. The NMR T_2 spectra of sample Sy18 exhibit this characteristic.

In the NMR measurements, no water signal was detected and only oil was detected. The differences in the NMR T_2 spectra represent the differences in the oil phase saturation before and after water flooding, reflecting the displacement effect [41, 42]. Figure 13 shows that there is a positive correlation between the displacement efficiency and the variation in the amplitude of the peak area of the T_2 spectrum before

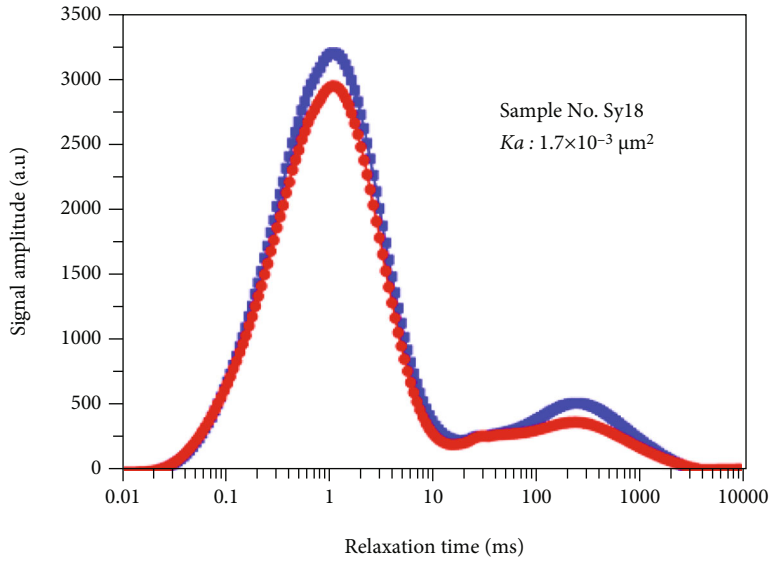

(a)

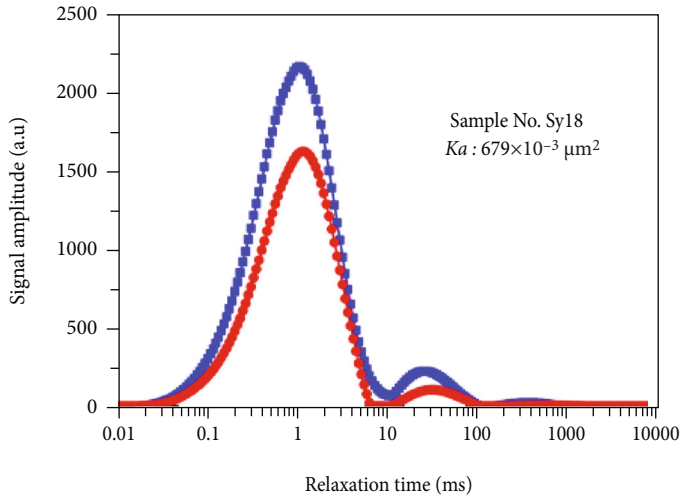

(b)

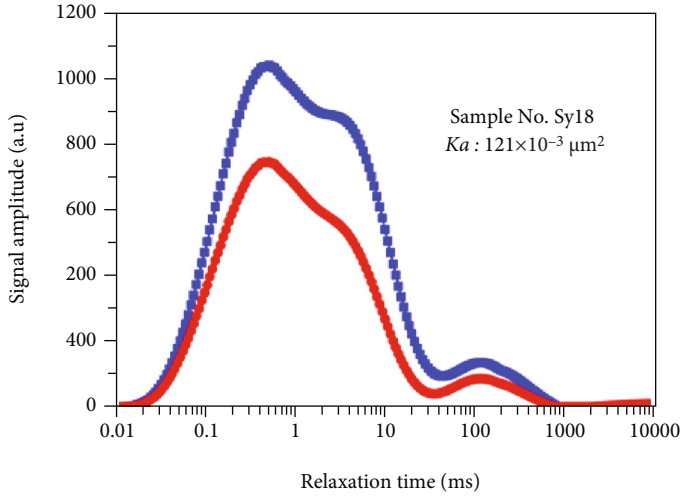

(c)

Figure 12: Continued.

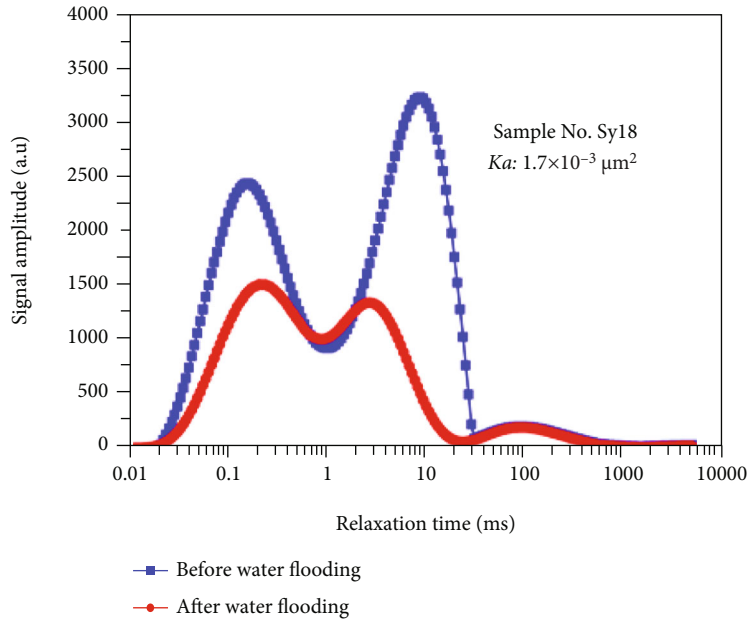

(d)

Figure 12: NMR T_2 spectra before and after water flooding. The red line represents the T_2 spectrum before water flooding, and the blue line represents that after water flooding.

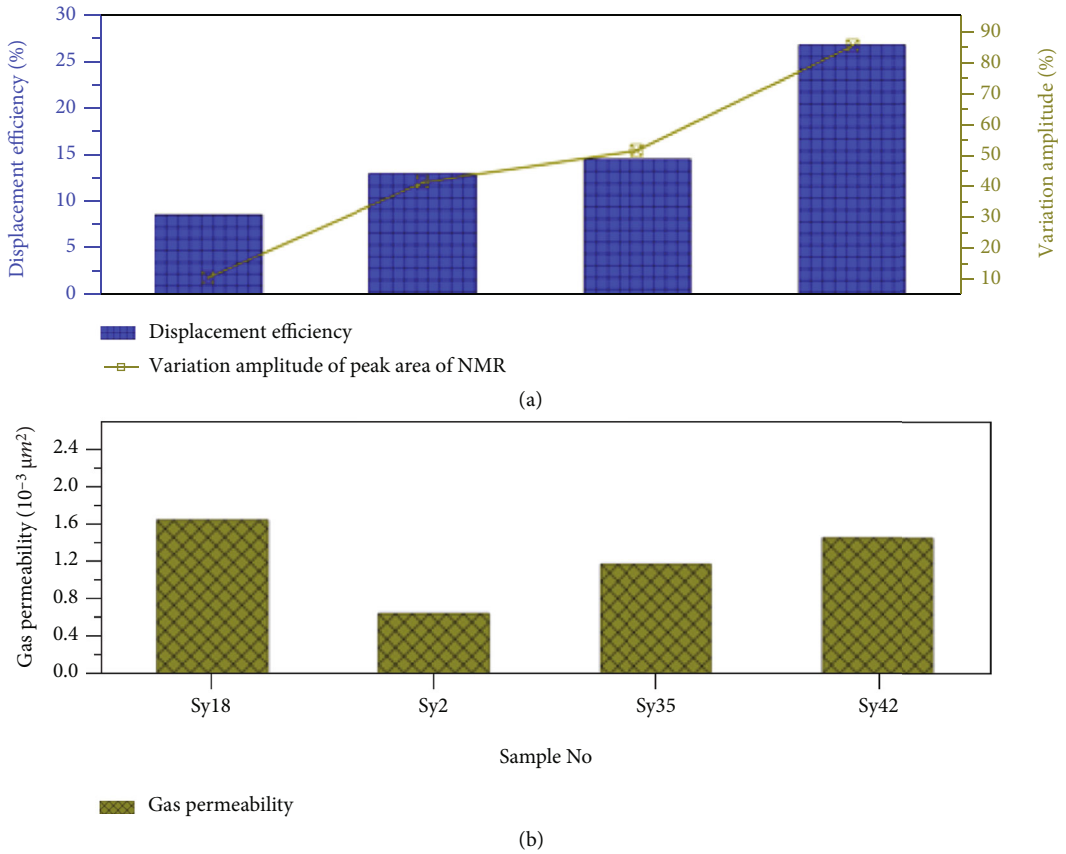

Figure 13: The relationships between the displacement efficiency and the variation in the amplitude of the peak area of the NMR before and after water flooding.

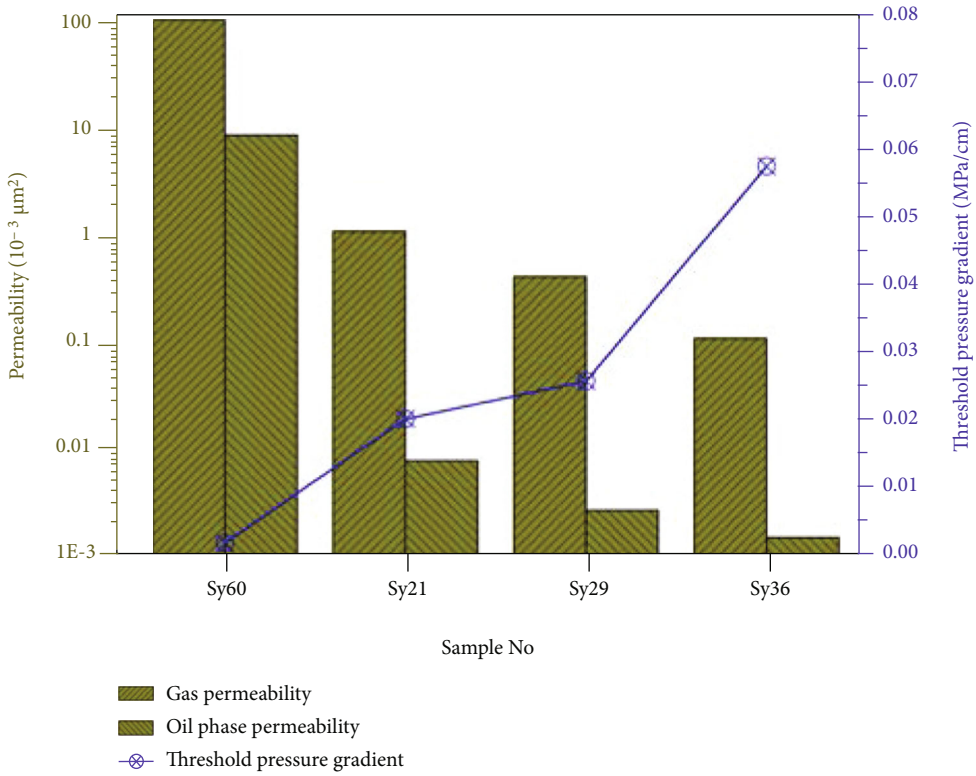

Figure 14: The relationship between the threshold pressure gradients and the air permeabilities of the core samples.

and after water flooding. In addition, as can be seen from Figure 13, there is no obvious correlation between the gas permeability and the displacement efficiency or the variation in the amplitude of the peak area. As can be seen from Figure 12, the peak of the T_2 spectrum after water flooding is lower than that before water flooding. In contrast, before and after water flooding, the T_2 spectrum of the matrix pore core exhibits more noticeable changes. This suggests that the matrix core has a good oil displacement effect.

4. Discussion

4.1. Stress-Sensitive Mechanism. For the fractured cores, under the simulated effective formation stress, the oil phase permeability at low pressure dropped significantly faster as the effective stress increased. The oil phase permeability decreased slowly in the high-pressure section. According to the results of previous studies, the stress-sensitive mechanism of the reservoir is controlled by the pore structure, mineral composition, etc. The flow channels in this type of core are microfractures (Figure 6(c)). The fractures have conjugate characteristics, and their connectivity is very good (Figure 6(b)). There are micro/nano- and microfractures, but the micropores are mainly nanoscale pores, in which fluid flow is difficult. The fluid mainly flows in the microfractures. The micropores are carbonate and clay mineral intergranular pore, and there are few large dissolution pores (Figures 6(a) and 6(f)). The microfractures closed first as the stress increased, and thus, the oil phase permeability decreased rapidly. As the stress continued to increase, it mainly affected the connectivity of the micropores. Because the carbonate intercrystalline pores have a strong supporting capacity and are not easily compressed, their stress sensitivity is completely different from that of the microfractures. This led to a slower decrease in the permeability. In other words, the stress sensitivity of carbonate reservoirs, especially the fractured reservoir in the Yingxi region, is strong. This may be one of the reasons for the rapid decline in the well yield.

4.2. Threshold Pressure Gradient. In general, the fluid flow in medium-to-high permeability porous media obeys Darcy's law. However, in low permeability tight reservoirs, the fluid flow is usually classified as low velocity non-Darcy flow. In this study, the lacustrine carbonate reservoir in the Yingxi area is a low permeability tight reservoir. The flow process exhibits non-Darcy flow characteristics. According to previous theoretical and laboratory studies, low velocity non-Darcy flow mainly results from tight pores and a boundary layer [19, 21]. It is generally acknowledged that low velocity non-Darcy flow is affected by the interaction forces between the fluid and the tight pores for small pressure gradients and low velocities [18]. The fluid in a porous medium can be divided into internal free fluid and boundary fluid. The boundary fluid has a higher density and viscosity and is the main cause of the nonlinear flow in low permeability tight reservoirs. The smaller the pore size is, the stronger the rock-fluid interactions are [43]. The lacustrine carbonate reservoir in the Yingxi area contains a large number of micro- and nanointercrystalline pores and dissolution pores. When crude oil flows through these smaller pore throats, a boundary layer is inevitably produced. In the early stages

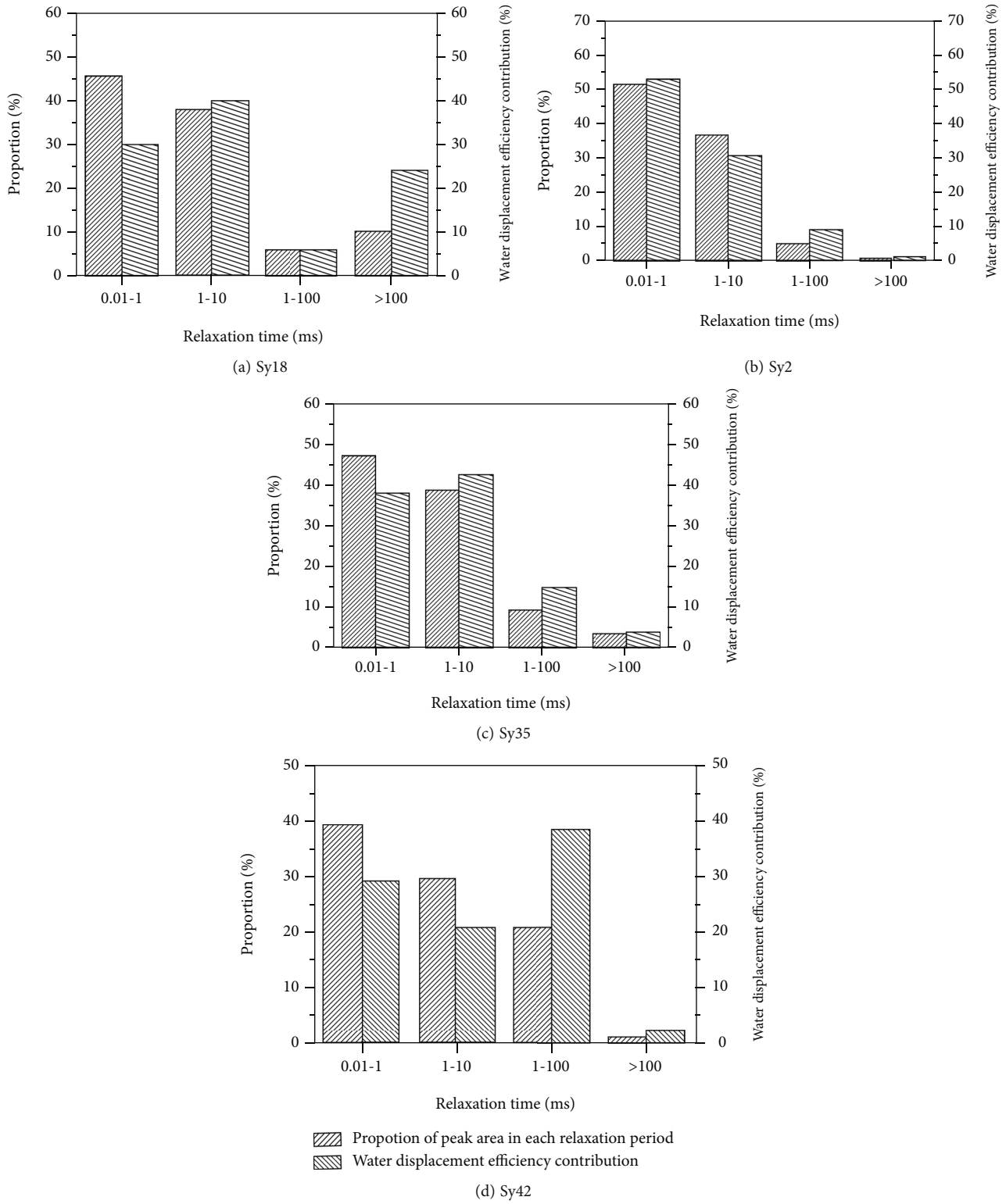

Figure 15: Proportions of the NMR peak area and the water displacement efficiency contribution for different relaxation times.

of development, the reservoir's pressure is very high, the pressure gradient is larger, and the permeability of the reservoir is large, and thus, the oil wells have high productions. As the formation pressure drops, the permeability of the reservoir also decreases due to its stress sensitivity. In addition, the non-Darcy flow is obvious, and some of the crude oil in the pore throats even fails to flow. Thus, the oil well production is affected by these two factors and exhibits a rapid decline. The threshold pressure gradient has important guiding significance for oilfield development. In addition, the threshold pressure gradient obtained in this study is 0.00216–0.0579 MPa/cm. Diwu et al. [18] calculated a

pseudo-total produced gas (TPG) of 0.104 MPa/m for a homogeneous model with artificial fracturing and an average permeability of 11 mD. The results for a typical well obtained using the numerical method revealed a close pseudo-TPG value of 0.27 MPa/m [35]. These values are close to the lower bound (0.00216 MPa/cm) in this study. Another comparison can be made with the TPG values reported by Yan et al. [44], i.e., a TPG of 0.15–3.5 MPa/m for $K = 0.3 - 10$ mD. The lower bound (0.15 MPa/m) is close to the lower bound (0.00216 MPa/cm) in this study. However, the upper bound in this study (0.0579 MPa/cm) is higher than their upper bound (3.5 MPa/m). This is reasonable because the permeability in our experiment (0.115 mD) is smaller than their lower bound (0.3 mD). The above comparison validates the ability of the proposed method to calculate the threshold pressure gradient. The physical properties have a great effect on the threshold pressure gradient. As can be seen from Figure 14, there is a certain correlation between the threshold pressure gradient and the air permeability of the core samples, i.e., the larger the air permeability, the smaller the threshold pressure gradient.

4.3. Oil and Water Displacement Characteristics. It should be noted that one of the main questions regarding water flooding is where the oil and water displacement occurs. In other words, we need to obtain a clear understanding of which pores play a major role. The variations in the peak area at different relaxation times before and after water flooding are different. Thus, the contribution rate of the water flooding at different relaxation times is also significantly different. In this study, the relaxation times were divided into four stages. The proportion of the difference in the peak area in each stage is defined as the contribution rate of the water flooding. The relaxation times in the range of 0.1–10 ms made the greatest contribution to the water flooding efficiency in these core samples (Figure 15). Thus, a fixed T_2 value can be related to the pore size directly [40, 45]. As discussed previously, T_2 components ranging from 0.1 ms to 10 ms are related to the <10 μm pores. In other words, the <10 μm intracrystalline and intergranular pores play a major role in the oil and water displacement.

Fractures can play an important role in the fluid storage–migration properties of carbonate reservoir [46–48]. The oil-water two-phase flow experiments revealed that during water flooding, the water permeability of the fractured cores increased rapidly, and the water flow capacity was strong; however, the effect of the water flooding was poor. The reason for this is that after the water phase enters the fractured cores, it flows along the fractures and a little may enter the large or small pores connected with the fractures. The limited amount of the oil phase in the micropores is displaced. Yang et al. [2] conducted experiments on water injection optimization for fractured-vuggy carbonate reservoirs. They proposed the use of water flooding because the heterogeneous connections between the fractures and vugs formed the dominant water flow pathways in some of the fracture channels. The water flowing through these channels only displaced part of the oil in the connected vugs. When the water phase flowed in the matrix core, although the flow was relatively slow, the water phase spread to more of the oil in the porous medium, and the effect of the water flooding was better. As shown in Figure 12, the micropores smaller than 10 μm in diameter play an important role in the water flooding of the matrix core. In contrast, for the fractured cores, the contribution of the micropores smaller than 10 μm in diameter to the water flooding is weak. Thus, for the fractured cores, it is essential to start up the residual oil in the micropores.

5. Conclusions

In this study, lacustrine carbonate rocks from the Yingxi area of the Qaidam Basin were investigated. This study was aimed at determining the flow mechanism of the carbonate reservoir under reservoir conditions. According to the comprehensive characterization of the rock samples, the pore structure was classified into two types: fractures and matrix pores. The fluid flow experiments under reservoir conditions showed that the reservoir has a threshold pressure gradient, and the flow does not obey Darcy's law due to the interaction forces between the fluid and the tight pores. There is a certain correlation between the threshold pressure gradients and the air permeabilities of the core samples. The permeabilities of the fractured cores decreased faster than those of the matrix pore cores with increasing effective stress. The type of pore structure has a significant effect on the oil-water two-phase flow. The water phase relative permeability when there is residual oil in the fractured core is higher than that of the matrix pore core. There is a positive correlation between the displacement efficiency and the variation in the amplitude of the peak area of the T_2 spectra before and after water flooding. Before and after water flooding, the T_2 spectra of the matrix pore cores exhibited noticeable changes, and they had a good oil displacement effect. For the matrix cores, the oil phase in a large number of the small pores was displaced. For the fractured cores, it is essential to start up the residual oil in micropores less than 10 μm in diameter.

Data Availability

The data used to support the findings of this study have not been made available because the data came from the test and analysis project of the oil field company, which was classified.

Conflicts of Interest

The authors declare that they have no conflicts of interest.

Acknowledgments

This research was funded by the National Natural Science Foundation of China (Grant No. 51741407), the Project of the Shaanxi Province Natural Science Basic Research Program (Grant No. 2021JQ-599), and the National Major Research Program for Science and Technology of China (Grant No. 2016ZX05050006). The authors acknowledge

the Shaanxi Key Laboratory of Advanced Stimulation Technology for Oil & Gas Reservoirs, School of Petroleum Engineering, Xi'an Shiyou University, for supporting this research.

References

[1] Y. Li, *Development Theories and Methods of Fracture-Vug Carbonate Reservoirs*, Academic Press, London, 2017.

[2] B. Yang, J. He, D. Lyu et al., "Production optimization for water flooding in fractured-vuggy carbonate reservoir–from laboratory physical model to reservoir operation," *Journal of Petroleum Science and Engineering*, vol. 184, p. 106520, 2020.

[3] Z. Xia, Z. Liu, S. Li, Y. Wang, and B. Guan, "Origin and developing model of rock salt: a case study of Lower Ganchaigou Formation of Paleogene in the west of Yingxiong ridge, Qaidam Basin," *Acta Petrolei Sinica*, vol. 38, no. 1, pp. 55–66, 2017.

[4] Y. S. Zhang, K. Y. Wu, Y. H. Jiang et al., "Geological characteristics of deep carbonate hydrocarbon-bearing pool in the western Yingxiongling area in Qaidam Basin," *Natural Gas Geoscience*, vol. 29, no. 3, pp. 358–369, 2018.

[5] Y. S. Zhang, Y. Q. Yang, Z. X. Qi, Y. D. Qiao, and H. R. Yuan, "Sedimentary characteristics and environments of the salt-bearing series of Qianjiang formation of the paleogene in Qianjiang sag of Jianghan Basin," *Journal of Palaeogeography*, vol. 5, no. 1, pp. 29–35, 2003.

[6] R. T. Guo, D. D. Ma, Y. S. Zhang et al., "Characteristics and formation mechanism of overpressure pore-fracture reservoirs for Upper Member of Xiaganchaigou Formation in the west of Yingxiong ridge, Qaidam Basin," *Acta Petrolei Sinica*, vol. 40, no. 4, pp. 411–422, 2019.

[7] J. Yuan, C. Huang, F. Zhao, and X. Pan, "Carbon and oxygen isotopic compositions, and palaeoenvironmental significance of saline lacustrine dolomite from the Qaidam Basin, Western China," *Journal of Petroleum Science and Engineering*, vol. 135, pp. 596–607, 2015.

[8] S. T. Fu, D. W. Zhang, and J. Q. Xue, "Exploration potential and geological conditions of tight oil in the Qaidam Basin," *Acta Sedimentologica Sinica*, vol. 31, no. 4, pp. 672–682, 2013.

[9] C. Huang, H. Chang, J. Cui, Y. Li, and L. Wu, "Oligocene sedimentary characteristics and hydrocarbon accumulation model in the western Qaidam Basin," *Acta Petrolei Sinica*, vol. 38, no. 11, pp. 1230–1243, 2017.

[10] S. M. Agar and G. J. Hampson, "Fundamental controls on flow in carbonates: an introduction," *Petroleum Geoscience*, vol. 20, no. 1, pp. 3–5, 2014.

[11] L. Wei, C. Shi, C. Yang, and L. Liu, "Classification and application of flow units in carbonate reservoirs," *IOP Conference Series: Earth and Environmental Science*, vol. 186, no. 3, 2018.

[12] M. Yang, H. Zhong, and Y. Li, "Research on fluid flow mechanism of fracture-cave carbonate reservoirs based on fluid mechanics," *Energy Sources, Part A: Recovery, Utilization and Environmental Effects*, vol. 5, pp. 1–19, 2020.

[13] Y. Yang, H. Q. Liu, J. Wang, Z. Zhang, Q. Chen, and H. Cheng, "Determination of flow units in carbonate reservoir with multiscale karst morphology," *Journal of Energy Resources Technology*, vol. 138, no. 3, 2016.

[14] H. F. Zhao, M. Chen, Y. Jing, Y. H. Ding, and Y. H. Wang, "Scale model of stress sensitivity for low permeability fractured reservoirs," *Acta Physica Sinica*, vol. 3, no. 1, pp. 7–12, 2015.

[15] R. Zhang, Z. F. Ning, H. S. Zhang, and Q. Xie, "New insights and discussions on stress sensitivity of fractured tight reservoir," *Natural Gas Geoscience*, vol. 27, no. 5, pp. 918–923, 2016.

[16] A. Fumagalli, L. Pasquale, S. Zonca, and S. Micheletti, "An upscaling procedure for fractured reservoirs with embedded grids," *Water Resources Research*, vol. 52, no. 8, pp. 6506–6525, 2016.

[17] P. Zuloaga-Molero, W. Yu, Y. Xu, K. Sepehrnoori, and B. Li, "Simulation study of CO_2-EOR in tight oil reservoirs with complex fracture geometries," *Scientific Reports*, vol. 6, no. 1, pp. 1–11, 2016.

[18] P. Diwu, T. Liu, Z. You, B. Jiang, and J. Zhou, "Effect of low velocity non-Darcy flow on pressure response in shale and tight oil reservoirs," *Fuel*, vol. 216, pp. 398–406, 2018.

[19] Y. M. He, X. C. Chen, Y. Zhang, and W. Yu, "Modeling interporosity flow functions and shape factors in low-permeability naturally fractured reservoir," *Journal of Petroleum Science and Engineering*, vol. 156, pp. 110–117, 2017.

[20] M. Kutiĺek, "Non-darcian flow of water in soils-laminar region: a review," *Developments in Soil Science*, vol. 2, pp. 327–340, 1972.

[21] C. Xu, Y. Kang, L. You, and Z. You, "Lost circulation control for formation damage prevention in naturally fractured reservoir: mathematical model and experimental study," *SPE Journal*, vol. 22, no. 5, pp. 1654–1670, 2017.

[22] B. Q. Zeng, L. S. Cheng, and C. L. Li, "Low velocity non-linear flow in ultra-low permeability reservoir," *Journal of Petroleum Science and Engineering*, vol. 80, no. 1, pp. 1–6, 2011.

[23] H. Daigle, B. Thomas, H. Rowe, and M. Nieto, "Nuclear magnetic resonance characterization of shallow marine sediments from the Nankai Trough, Integrated Ocean Drilling Program Expedition 333," *Journal of Geophysical Research, Solid Earth*, vol. 119, no. 4, pp. 2631–2650, 2014.

[24] J. Lai, G. Wang, Z. Fan et al., "Insight into the pore structure of tight sandstones using NMR and HPMI measurements," *Energy & Fuels*, vol. 30, no. 12, pp. 10200–10214, 2016.

[25] L. O. Pires, A. Winter, and O. V. Trevisan, "Dolomite cores evaluated by NMR," *Journal of Petroleum Science and Engineering*, vol. 176, pp. 1187–1197, 2019.

[26] B. Vincent, M. Fleury, Y. Santerre, and B. Brigaud, "NMR relaxation of neritic carbonates: an integrated petrophysical and petrographical approach," *Journal of Applied Geophysics*, vol. 74, no. 1, pp. 38–58, 2011.

[27] A. F. Li, M. Liu, S. H. Zhang, and J. Yao, "Experimental study on the percolation characteristic of extra low-permeability reservoir," *Journal of Xi'an Shiyou University*, vol. 23, no. 2, pp. 35–39, 2008.

[28] B. D. Lowden, M. J. Porter, and L. S. Powrie, "T_2 relaxation time versus mercury injection capillary pressure: implications for NMR logging and reservoir characterisation," in *SPE European Petroleum Conference*, pp. 323–334, Hague, Netherlands, 1998.

[29] H. Gao, Y. L. Liu, Z. Zhang, B. L. Niu, and H. Z. Li, "Impact of secondary and tertiary floods on microscopic residual oil distribution in medium-to-high permeability cores with NMR technique," *Energy & Fuels*, vol. 29, no. 8, pp. 4721–4729, 2015.

[30] H. B. Li, J. Y. Zhu, and H. K. Guo, "Methods for calculating pore radius distribution in rock from NMR T_2 spectra," *Chinese Journal of Magnetic Resonance*, vol. 25, no. 2, pp. 273–280, 2008.

[31] X. X. Li, X. J. Ren, J. Tian, and H. H. Ma, "Pore characteristics and their influences on the water-oil flow for Reservoir Chang-8 in Dingbian Block X," *Petroleum Geology & Oilfield Development in Daqing*, vol. 39, no. 1, pp. 41–49, 2020.

[32] J. Lai, S. Wang, C. Zhang et al., "Spectrum of pore types and networks in the deep Cambrian to Lower Ordovician dolostones in Tarim Basin," *Marine and Petroleum Geology*, vol. 112, 2020.

[33] A. Prada and F. Civan, "Modification of Darcy's law for the threshold pressure gradient," *Journal of Petroleum Science and Engineering*, vol. 22, no. 4, pp. 237–240, 1999.

[34] Y. E. Deng and C. Q. Liu, "Mathematical model of nonlinear flow law in low permeability porous media and its application," *Acta Petrologica Sinica*, vol. 23, no. 4, pp. 72–77, 2001.

[35] D. L. Li, W. S. Zha, S. F. Liu, L. Wang, and D. T. Lu, "Pressure transient analysis of low permeability reservoir with pseudo threshold pressure gradient," *Journal of Petroleum Science and Engineering*, vol. 147, pp. 308–316, 2016.

[36] Y. Shi, Z. M. Yang, and Y. Z. Huang, "Study on non-linear seepage flow model for low-permeability reservoir," *Acta Petrologica Sinica*, vol. 30, no. 5, pp. 731–734, 2009.

[37] X. K. Wang and J. J. Sheng, "Effect of low-velocity non-Darcy flow on well production performance in shale and tight oil reservoirs," *Fuel*, vol. 190, pp. 41–46, 2017.

[38] S. T. Bai, D. J. Cheng, J. B. Wan et al., "Quantitative characterization of sandstone NMR T_2 spectrum," *Acta Petrologica Sinica*, vol. 37, no. 3, pp. 382–391, 2016.

[39] W. F. J. Slijkerman, J. P. Hofman, W. J. Looyestijn, and Y. Volokitin, "A practical approach to obtain primary drainage capillary pressure curves from NMR core and log data," *Petrophysics*, vol. 42, no. 4, pp. 334–343, 2001.

[40] J. Lai, S. Wang, G. Wang et al., "Pore structure and fractal characteristics of Ordovician Majiagou carbonate reservoirs in Ordos Basin, China," *AAPG Bulletin*, vol. 103, no. 11, pp. 2573–2596, 2019.

[41] X. Dong, L. W. Shen, X. Liu et al., "NMR characterization of a tight sand's pore structures and fluid mobility: an experimental investigation for CO_2 EOR potential," *Marine and Petroleum Geology*, vol. 118, 2020.

[42] X. F. Liu, X. Dong, N. Golsanami et al., "NMR characterization of fluid mobility in tight sand: analysis on the pore capillaries with the nine-grid model," *Journal of Natural Gas Science and Engineering*, vol. 94, 2021.

[43] S. L. Xu, X. A. Yue, J. R. Hou, and B. X. Wang, "Influence of boundary-layer fluid on the seepage characteristic of low-permeability reservoir," *Journal of Xi'an Shiyou University*, vol. 22, no. 2, pp. 26–28, 2007.

[44] M. Yan, C. Wu, and Y. Wang, "Tendency of starting pressure gradient changes in heterogeneous reservoirs," *Journal of Oil and Gas Technology*, vol. 28, no. 3, pp. 129-130, 2006.

[45] A. Dillinger and L. Esteban, "Experimental evaluation of reservoir quality in Mesozoic formations of the Perth Basin (Western Australia) by using a laboratory low field nuclear magnetic resonance," *Marine and Petroleum Geology*, vol. 57, pp. 455–469, 2014.

[46] F. Agosta, M. Alessandroni, M. Antonellini, E. Tondi, and M. Giorgioni, "From fractures to flow: a field-based quantitative analysis of an outcropping carbonate reservoir," *Tectonophysics*, vol. 490, no. 3-4, pp. 197–213, 2010.

[47] S. Zendehboudi, I. Chatzis, A. A. Mohsenipour, and A. Elkamel, "Dimensional analysis and scale-up of immiscible two-phase flow displacement in fractured porous media under controlled gravity drainage," *Energy & Fuels*, vol. 25, no. 4, pp. 1731–1750, 2011.

[48] S. Zendehboudi, I. Chatzis, A. Shafiei, and M. B. Dusseault, "Empirical modeling of gravity drainage in fractured porous media," *Energy & Fuels*, vol. 25, no. 3, pp. 1229–1241, 2011.